The Meteoritical Society

Meteoritics & Planetary Science 59, Nr 3, 544–559 (2024)
doi: 10.1111/maps.14138

Polygonal impact craters on Ganymede

Namitha Rose BABY [1,2]*, Thomas KENKMANN [2], Katrin STEPHAN [1], and Roland WAGNER [1]

[1]Deutsches Zentrum für Luft- und Raumfahrt (DLR), Berlin, Germany
[2]Institut für Geo- und Umweltnaturwissenschaften, Universität Freiburg, Freiburg im Breisgau, Germany
***Correspondence**
Namitha Rose Baby, Deutsches Zentrum für Luft- und Raumfahrt (DLR), Berlin, Germany.
Email: namitha.baby@dlr.de

(Received 20 June 2023; revision accepted 05 January 2024)

Abstract–Polygonal impact craters (PICs) are unique geological features observed on various planetary bodies and constitute a small percentage of the impact crater population. This study focuses on PICs on Ganymede, where no such craters have been investigated so far. Here we present the distribution of PICs, examine their morphological characteristics, investigate the causes for their polygonal shapes, and discuss the factors that support their formation. We identified and analyzed 459 PICs on Ganymede with complex crater morphologies. They are widely distributed across the Moon and occur on both dark and light terrain. Our analysis revealed that the majority of orientations of straight rim segments align parallel or subparallel to adjacent tectonic linear features. There is at least one tectonic linear orientation adjacent to PICs, even in dark, cratered terrains. Based on the comparison of the number of PICs and tectonic linear features, Ganymede is believed to have undergone more intense tectonic activity than other icy bodies like Ceres and Dione, where PICs were described. The presence of numerous PICs on Ganymede suggests that surface lineations and grooves are expressions of fractures that form zones of weakness in the ice crust that got reactivated during impact cratering.

INTRODUCTION

Ganymede's Geology

Ganymede, the largest planetary satellite of the solar system, is a differentiated icy moon with an inner rocky core, an icy mantle with different layers that are believed to be liquid, and an icy crust. The bulk composition of Ganymede is comprised of approximately 60% rock and 40% ice (Pappalardo et al., 2004). Approximately 35% of the surface is densely cratered, low albedo area, known as dark terrain. It is considered to represent the oldest preserved surface. This terrain is crosscut by tectonically active, younger, brighter, and less densely cratered terrain called light terrain, which constitutes approximately 65% of the surface (Collins, 2000; Schenk et al., 2001; Shoemaker et al., 1982). The light terrain is sculptured by grooves and ridges to various degrees. The aligned features are believed to represent fault scarps of normal faults and graben structures, but some have been formed by strike-slip transpressional and transtensional faulting. Lineated light terrain may also have formed by some sort of spreading (Collins et al., 1998). Owing to its relief, the light terrain can be subdivided into several subunits with slightly different crater densities (Baby et al., 2023). Dark terrain is mainly found as cratered terrain, while in some regions it is also highly lineated. These dark lineated terrains have intermediate ages between those of the dark cratered terrain and the light terrain and may indicate the beginning of extensional faulting and break-up of the dark terrain (Baby et al., 2023; Patterson et al., 2010). The major tectonic features observed on dark terrain are furrows, which are interpreted as remnants from large impact events (Hirata et al., 2020; Schenk & McKinnon, 1987; Zuber & Parmentier, 1984), and minor tectonic features in the form of fractures (Rossi et al.,

2023). It is believed that a large number of impact craters were destroyed during resurfacing activities on Ganymede.

Polygonal Impact Craters

Polygonal impact craters (PICs) have at least one straight rim segment in planform (Beddingfield et al., 2016; Beddingfield & Cartwright, 2020). Studies distinguishing PICs from circular impact craters go back to the 1960s. PICs constitute a small fraction of all impact craters, and they exist on both rocky and icy planetary bodies of the solar system (Öhman et al., 2010). For example, on Earth, 208 impact craters were discovered and confirmed so far (Gottwald et al., 2020; Kenkmann, 2021). Among those, 14 craters, or 7%, were identified as PICs, including the well-known quadrangular Meteor Crater of Arizona (Kumar & Kring, 2008; Poelchau et al., 2009; Shoemaker, 1963) and the hexagonal Söderfjärden crater of Finland (Abels, 2003; Gottwald et al., 2020; Talvitie et al., 1975).

PICs on Icy Bodies in the Asteroid Belt and Outer Solar System

PICs have been reported from the asteroid Ceres and many icy bodies of the outer solar system (e.g., Buczkowski et al., 2016; Porco et al., 2005). Ceres has a low albedo surface that is enriched in ammoniated phyllosilicates, salts, and organics (De Sanctis et al., 2015; Stephan et al., 2019) and is assumed to host significant amounts of water ice in its subsurface (Prettyman et al., 2017). Ceres shows a larger number of PICs in its northern hemisphere in comparison to the southern latitudes (Otto et al., 2016). PICs on Ceres mainly have hexagonal shapes with their adjacent straight rim segments subtending an average angle of about 121.99° (Zeilnhofer & Barlow, 2021). During the Voyager missions, PICs were identified on numerous icy moons in the outer solar system. A detailed study on PICs was done during the Galileo and Cassini missions. Of the Jovian satellites, Callisto shows small craters with diameters of 7 km and less that have polygonal shapes in planform. They exhibit a range of degradation states, starting from simple-bowl-shaped fresh craters, which often have high-albedo ejecta to highly eroded craters with discontinuous rims and a lack of ejecta blanket (Greeley et al., 2000). On Europa, the largest and youngest crater, Amergin of the trailing hemisphere, has a polygonal shape that is controlled by preexisting tectonic linear features in that area (Figueredo & Greeley, 2004). To our knowledge, PICs have not been reported from Ganymede so far.

Fresh craters of the Saturnian moon Rhea were identified to have strong polygonal outlines (Moore et al., 1985; Smith et al., 1981). PICs on Tethys show the highest concentration in/near Ithaca Chasma, which is indicative of a high degree of subsurface fracturing (Ferguson et al., 2020). On Dione, many of the craters identified from Voyager data have polygonal rims (Moore, 1984). A detailed study by Beddingfield et al. (2016) showed that PICs are abundant both within the wispy and non-wispy terrains, whereas in the non-wispy terrain, a lesser number of fractures were found. PICs were also identified on Iapetus (Denk et al., 2005; Porco et al., 2005; Singer & McKinnon, 2011). In the case of Titan, the Selk crater appears polygonal in outline, and its two straight rim segments have azimuths that align parallel to the planes of weakness that existed in the crust prior to the existence of the crater (Soderblom et al., 2010). On Enceladus, square-shaped PICs (2 km in diameter) were observed in subdued cratered plains of the north polar region, where the subdued troughs aligned parallel with straight rim segments of these PICs (Crow-Willard & Pappalardo, 2015). Through examination of Mima's global mosaic, PICs were identified, though they remain unstudied to date.

On the Uranian moon Miranda, 14 PICs were confirmed and identified as an important indicator of subtle and non-visible fracture systems (Beddingfield & Cartwright, 2020). On Ariel, many of the craters are polygonal in outline, and their straight segments trend parallels the major structural trends (Plescia, 1987). On Oberon, many of the craters with diameters of less than 100 km were identified as polygonal in shape (e.g., the large crater Hamlet; Plescia, 1987). The lack of sufficient data for Umbriel and Titania limited detailed studies on them. However, since both are highly cratered and contain lineated features like the other Uranian moons, the chances for finding PICs are not negligible. On Charon, Pluto's companion, PICs are present within the fractured and rilled terrain of Vulcan Planitia, as well as to the north and south, in close proximity to Clark Montes. Additionally, PICs have been identified to the east of Kubrick Mons, where the straight rim segments run parallel to the fracture systems in that area (Beddingfield et al., 2020). All the above examples suggest that PICs are common on most of the celestial bodies of outer solar system.

Possible Models for PIC Formation

Deviations from a circular shape for any impact crater depend on either the angle of impact, the velocity of the impacting body, the size and shape of the impacting body, and/or target body heterogeneity (Eppler et al., 1983). Additionally, the topography of target body, particularly, impacting into slope can give rise to asymmetrical craters (Aschauer & Kenkmann, 2017).

Earlier Works on Formation Mechanism for PICS

Ideally, vertical impacts of spherical object into homogenous target body would give rise to circular craters (Öpik, 1969). However, cratering tests conducted by Darling and Mes (1948) on basalt found that a joint fabric of the parent rock had control on the development of straight rim segments for the crater. Similarly, cratering experiments conducted on Buckboard Mesa at the Nevada Test Site into basaltic rocks resulted in PIC formation (Johnson, 1962). Later, an experiment conducted by Gault et al. (1968) at the NASA Ames Vertical Gun Range showed that crater impacted into a target with two perpendicular joint sets would give rise to square-shaped or hexagonal-shaped PIC, where its diagonals run parallel to the joints. All these laboratory experiments show that already-existing linear features of rock influence the rims of the crater when it is emplaced.

The effect of projectile shape on the final crater morphology is negligible compared to other factors such as impact angle, velocity, and target properties (Anderson et al., 2003; Pierazzo & Collins, 2004). For simple craters, the crater rim attains the straight rim segments during the excavation stage (Beddingfield et al., 2016; Eppler et al., 1983; Poelchau et al., 2009; Schultz, 1976; Watters et al., 2011). Poelchau et al. (2009) found that it is roughly 1.4 times easier to excavate a crater parallel to the joints than at 45° angle to the joint planes. This enlarges the transient cavity along the zones of weakness that trend along the diagonals of a quadrangular crater such as the Meteor Crater. The straight rim segments of such simple craters thus trend at 45° to the zones of weakness. In contrast to complex craters, the crater rim attains straight segments during the modification stage via slumping or normal faulting along the preexisting fractures within the crater wall (Beddingfield et al., 2016; Eppler et al., 1983; Schultz, 1976). Thus, the straight rim segments trend parallel to the crustal zones (joints, faults) of weakness. Due to the reduced spatial resolution of remote-sensed data on Ganymede, almost all described PICs belong to the group of complex craters, so that the polygonality should be governed by the crater modification stage rather than crater excavation.

Here we report on polygonal craters on Ganymede that have been discovered on both light and dark terrains. The presence of PICs is studied in relation to the linear features on the dark and light terrain. We will present the distribution of PICs across Ganymede, describe their morphological characteristics and their genetic relationship with tectonic linear features. The formation of PICs is discussed in the light of target material characteristics and gravitational influences.

METHODOLOGY

Data

For mapping PICs on the entire Ganymede surface, we used the new global mosaic, which combines the best high-resolution images from Voyager 1, Voyager 2, Galileo, and Juno spacecrafts (Kersten et al., 2022). Juno images were obtained on June 7, 2021, during Juno's closest approach with Ganymede at an altitude of 1044 km at the perijove 34 using a wide-angle camera (Hansen et al., 2022; Ravine et al., 2022). JunoCam captured comparatively better illuminated and slightly higher resolution images between longitudes 40°W and 25°E (1 km per pixel) than those obtained from Voyager 1 + 2 and Galileo spacecrafts (Hansen et al., 2022). So, the available global mosaic has integrated images with spatial resolutions starting from 100 m per pixel to 10 km per pixel (Kersten et al., 2021). We find that resolutions coarser 5 km per pixel are not sufficient to identify or digitize PICs. Images with extreme illumination conditions such as emission, incidence, and phase angles smaller than 15° and larger than 75° were excluded from this study in order to minimize effects onto the identification of PICs. Although images with relatively large illumination angles causing shadows still enable the identification of straight rims of PICs on Ganymede given the maximum topographic differences of 1 km, particularly smaller angles significantly reduce topographic image information and thus limit the investigation of characteristics of local surface features (Collins et al., 2013; Stephan et al., 2021).

PIC Identification and Analysis

We conducted a visual inspection of craters to identify potential straight sides as opposed to arcs within each crater. An edge that appears straight and terminates at a vertex point is deemed a straight rim segment. Therefore, a crater with multiple straight rim segments is characterized by distinct azimuths and separation by vertices. We mapped all the craters that have at least one straight rim segment in a plane view. Most of the previous studies considered PICs as those having at least two straight segments with an angle subtended between them (Aittola et al., 2010; Dasgupta et al., 2019; Neidhart et al., 2017; Öhman et al., 2008; Weber et al., 2022; Weihs et al., 2015; Zeilnhofer & Barlow, 2021). But since a single straight rim segment of a crater could also reveal the relationship with adjacent linear features, it is unavoidable to map them. This is supported by the studies from Beddingfield et al. (2016, 2020, 2022).

We identified and mapped 459 PICs across Ganymede. Those PICs, which were crosscut by other

craters or terrains, are not considered for the study. Mapped PICs have diameters ranging from 5 to 153 km. In regions, where the resolution is larger than 4 km per pixel, PICs identification was restricted to only those craters that have a somewhat larger diameter. PICs with 5 km diameter are mostly taken from the higher-resolution images whose resolution is better than 100 m per pixel. The crater rims were mapped manually using ArcGIS 10.7. To ensure accurate diameter measurement and minimize distortion during the analysis of straight rim segments, each of the PICs to be analyzed is projected in the center. For PICs in areas poleward of 60°, the global mosaic has been re-projected into stereographic projection and centered into each crater. For the other areas, mapping has been carried out in an equidistant cylindrical projection (Plate Carree projection). Morphometrical measurements like diameter, perimeter, area, azimuths, number of straight segments, and length of straight segments are measured using ArcGIS. Moreover, the orientation of lineations are determined in the vicinity of a crater. These geometrical measurements were obtained to characterize (i) the angularity, (ii) the maximum crater diameter for polygonality, and (iii) the dependence of straight rim orientation to the orientation of linear features.

Angularity is a measure of how much a polygon deviates from an ideal circular shape. In the case of impact craters, angularity refers to the degree to which the shape of the PIC deviates from that of an ideal circular impact crater with the same area as the polygon. It can be formulated as the following:

$$\text{Angularity} = \left(P_p/A_p\right)/\left(P_c/A_p\right)$$

where P_p is the perimeter of the polygonal crater, A_p is the area of the polygonal crater, and P_c is the perimeter enclosed if it is a circular crater.

The higher the angularity value, the more angular the polygon is, and hence the more it deviates from the expected circular crater shape. In general, the angularity of PICs depends on the number of sides, the length of each side, and the angles between the straight rim segments.

Rose diagrams were prepared with QGIS to statistically illustrate the orientation distribution of the straight rim segments of PICs. The major trend of straight rim segments in each of the PICs are discernible when applying weighting on the length. We utilized a bin count of 16, dividing the 360° circle into 16 equal intervals, each spanning 22.5°. In the case of a circular impact crater, the rose diagram also forms a circle, with all directions being nearly equal. But in the case of PICs, straight rim segments and their orientation are analyzed based on the longest directional value.

RESULTS

Morphology of PICs

Most of the mapped PICs on Ganymede deviate from ideal polygonal shapes. They are mostly seen as imperfect squares, pentagons, hexagons, etc. In other cases, some PICs have a few numbers of well-developed straight rim segments, and the rest of the sides appear more rounded in appearance. Figures 1 and 2 show typical examples of PICs observed on Ganymede and imaged by the Galileo spacecraft.

Achelous and Gula

Achelous is a 35-km-diameter fresh polygonal pedestal/rampart-like impact crater located at ~62°N, 12°W of the north pole side (Figure 1a). It is impacted on light-grooved terrain of Aquarius Sulcus. The availability of a high-resolution image of ~178 m per pixel enabled to study its polygonal morphology in detail. Its fluidized ejecta is radial in shape and has a radial extent of ~17 km (Boyce et al., 2010; Jones et al., 2003). Jones et al. (2003) suggested that it has a double-layered morphology, with the outer discontinuous ejecta deposited beyond the pedestal deposit. The continuous ejecta corresponds to the margin of a palimpsest. The double-layered nature results from the presence of near-surface target volatiles rather than atmospheric effects (Jones et al., 2003). Achelous has seven straight rim segments (Figure 1b). Gula is another ~35-km-diameter crater located north of Achelous. Unlike Achelous, it does not have any visible pedestal deposits surrounding it, while it is punctured by secondary craters emanating from Achelous. Gula has two straight rim segments, and other parts of the rim appear to be rounded in shape (Figure 1b). The rose diagrams display the major orientations of their straight rim segments with respect to adjacent linear features. The dominant orientation of the longest straight rim segments of Achelous and Gula is in E–W direction (Figure 1c,d). Three major light-grooved terrains are found in and near Achelous and Gula, and they are: older terrain unit lg_1, intermediate-aged lg_2, and the youngest lg_3 (the mapping scheme is followed from Patterson et al., 2010). The relative age determination is done based on the principle of cross-cutting relationship. Gula and Achelous are located on the oldest unit, lg_1, whose lineaments trend in a single direction, that is, in the NE–SW direction (Figure 1e). While the dominant orientation of lg_2 is in the NW–SE direction (Figure 1f), and lg_3 is in the NE–SW direction (Figure 1g). Among these seven straight rim segments, two of them align parallel with the lineaments, while the other five segments are at ~45° angle with rim segments that parallel the lineaments. Like Achelous, the lineaments adjacent to Gula also trend in the NE–SW

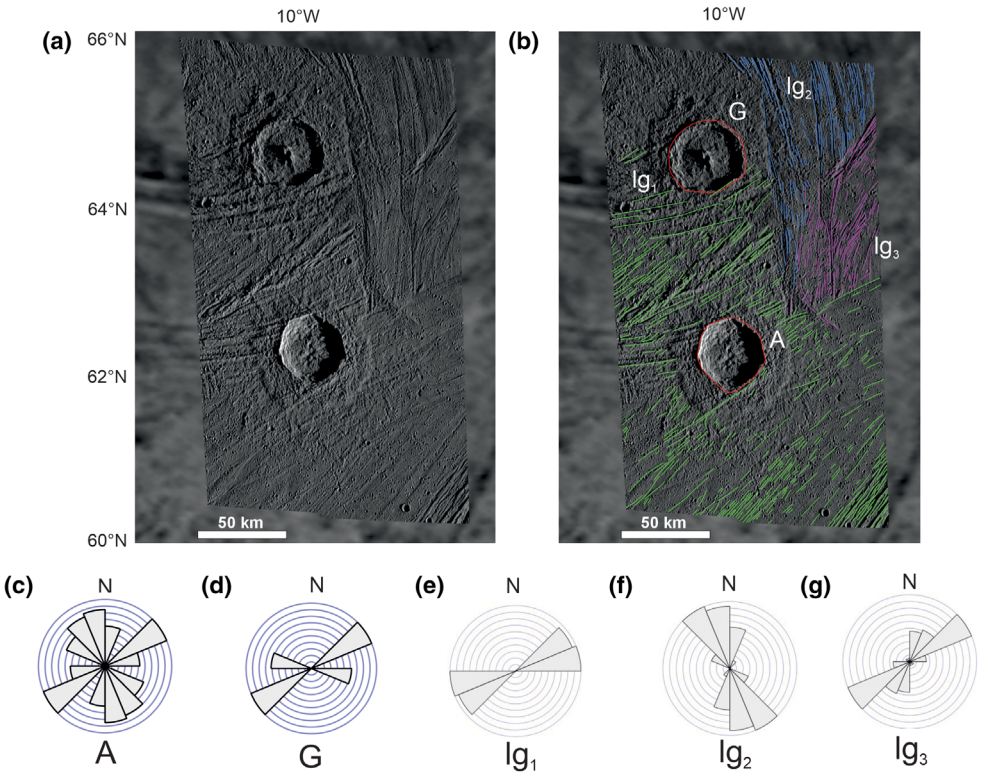

FIGURE 1. (a) SSI observation G7GSACHELS01 showing the PIC Achelous. (b) Lineament orientation mapping in the vicinity of PICs Achelous and Gula (red). "A" denotes Achelous, and "G" denotes Gula. (c) Rose diagrams showing the orientation of straight rim segments of Achelous and (d) Gula. (e) Rose diagram showing orientation of lineaments in terrain unit lg_1. (f) Rose diagram showing orientation of lineaments in terrain unit lg_2. (g) Rose diagram showing orientation of lineaments in terrain unit lg_3. Note that the names of the terrain units are followed according to the mapping scheme of Patterson et al. (2010). (Color figure can be viewed at wileyonlinelibrary.com)

direction. One of its straight rim segments clearly aligns parallel with the adjacent lineaments.

We found that there is no/negligible influence of the lg_2 and lg_3 lineaments in controlling their rim (Figure 1b). Namely, Gula is located at ~13 km away from the nearest lineament of lg_2, which clearly have not influenced much in the development of the straight rim segment. In terms of length, the longest ones are those straight rim segments that are parallel with the lineaments. There are no noticeable radial and circumferential fractures associated with PICs. Also, lineaments are found extending into the pedestal ejecta of Achelous, indicating the influence of lineaments.

Kittu

Kittu is a ~18-km-diameter PIC located in Ganymede's trailing hemisphere. The crater has a dark ejecta with a "butterfly wing" pattern extending for a long distance (Figure 2a), indicating a low impact angle <10°–15° with respect to the target surface (Melosh, 1989). Earlier studies suggested that it contains subsurface chondritic silicates, which got exposed during the impact event (Hartman, 1980). From spectral analysis, their dark ejecta was interpreted to contain more non-ice material and a higher concentration of CO_2 (Hibbitts et al., 2003).

The image of Kittu used for the study has a resolution of 145 m per pixel. Kittu is identified with six straight rim segments (Figure 2b), whose two longest straight segments have NW–SE orientation (Figure 2c). Kittu is emplaced at the border of two light grooved terrains lg_1 and lg_2 (mapping scheme followed from Patterson et al., 2010), where a major portion of the crater is placed onto the younger terrain unit lg_2. From this stratigraphic relationship, it is clear that Kittu represents the youngest unit. The lineaments in lg_2 trend in the NW–SE direction (Figure 2d), while lineaments in lg_1 trend in the NE–SW direction (Figure 2e).

The rose diagram of Kittu shows that the longest straight rim segments are the ones that are aligned parallel to the lineaments. Since Kittu is at the interface between two differently oriented terrains, we find the rims got aligned parallel with the ridges or grooves of both terrains. Usually, for a very oblique impact <15°m measured from the surface, an elliptical crater is formed, but here, where it is incident on grooved terrain, the elongation of the crater rim is obviously suppressed. There are no noticeable radial

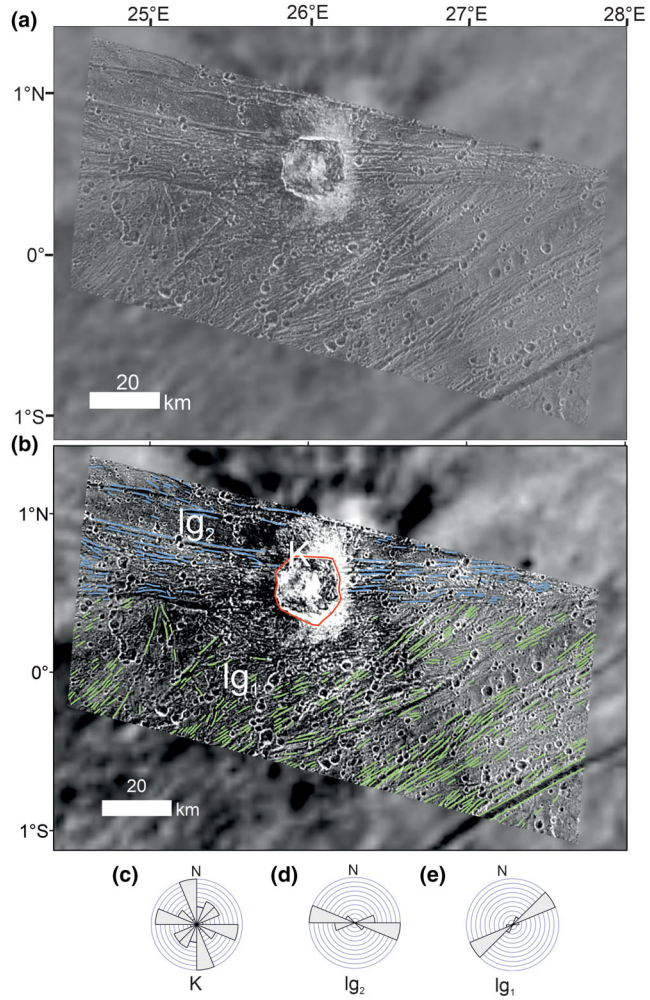

FIGURE 2. (a) SSI observation G7GSKITTU01 showing the PIC Kittu. (b) Lineament orientation mapping in the surrounding of PIC Kittu (K). (c) Rose diagram showing orientation of straight rim segments of Kittu. (d) Rose diagram showing the orientation of lineaments in terrain unit lg_2. (e) Rose diagram showing the orientation of lineaments in terrain unit lg_1. Note that the names of the terrain units are followed according to the mapping scheme of Patterson et al. (2010). (Color figure can be viewed at wileyonlinelibrary.com)

and circumferential fractures associated with this PIC. Also, secondary craters and bright ejecta restrict further analysis of its surroundings.

Distribution of Different Types of PICs across Ganymede

The mapped PICs show an uneven distribution across Ganymede (Figure 3). This is primarily caused by the lack of equally resolved remote sensing data. Because of this, PICs are hardly noticed in regions with resolutions of 5 km per pixel, which is the lowest resolution at which two PICs with diameters of 145 and 119 km are mapped. For instance, a very few PICs are mapped from regions 60°N and higher and longitudes between 60°E and 140°E (except regions down to 60°S).

Among the 459 PICs identified and mapped, about 215 (47%) were found on dark terrain, 210 on light terrain (46%), 33 bordering between dark and light terrain (7%), and 1 PIC on reticulate terrain (Figure 4). As the dark terrain covers 35% of Ganymede's surface, the number of PICs on this terrain appears high. However, one has to consider here that the average crater density is higher on dark terrain than on light terrain, increasing the absolute number of PICs.

With regard to the diameter, those craters between 20 and 40 km in diameter are most frequent among PICs, and they are equally present on dark and light terrains (Figure 4). This is the same with PICs found at borders between dark and light terrains. The number of PICs gradually decreases with increasing diameters. This, however, also reflects the circumstance that the absolute number of craters decreases with increasing diameter. The relatively low number of PICs with less than 20 km diameter is biased by resolutions of images that ranges from 100 m per pixel to lower than 4 km per pixel (Figure 4).

Most of the PICs identified have either a pit, a peak, or a dome as central features and fall in the category of complex craters (Figure 5). Among the 459 PICs identified and mapped, about 157 PICs' have a central peak, 124 of them have a pit, and five of them have a central dome. About 26 PICs were marked as "none," which expresses that any central feature is missing. However, these craters are too large to denote them as simple craters. About 147 PICs were marked as "unknown" whose central features were not able to be detected as peak, pit, or lack any central feature due to insufficient resolution. The maximum number of central peak PICs are found between 10 and 25 km in diameter and gradually decreases in number with increasing diameters. In contrast, PICs with a central pit are larger on average, and the maximum number is found between 45 and 85 km in crater diameter. Dome PICs are fewer in number, and their diameters start from 110 and larger. For PICs without discernable central feature, the diameters range between 20 and 60 km.

The largest detected PIC has a diameter of 153 km and has a dome as a central feature. The smallest detected PIC is 5 km in diameter and contains a central peak.

Number of Segments

Figure 6 shows the number of straight segments of the analyzed PICs. Polygonal craters with two straight segments are most frequent, followed by those with a hexagonal shape (6 segments). PICs with just one and nine linear segments are rare. Some of the analyzed craters have a square, pentagonal, or octagonal shapes, while others

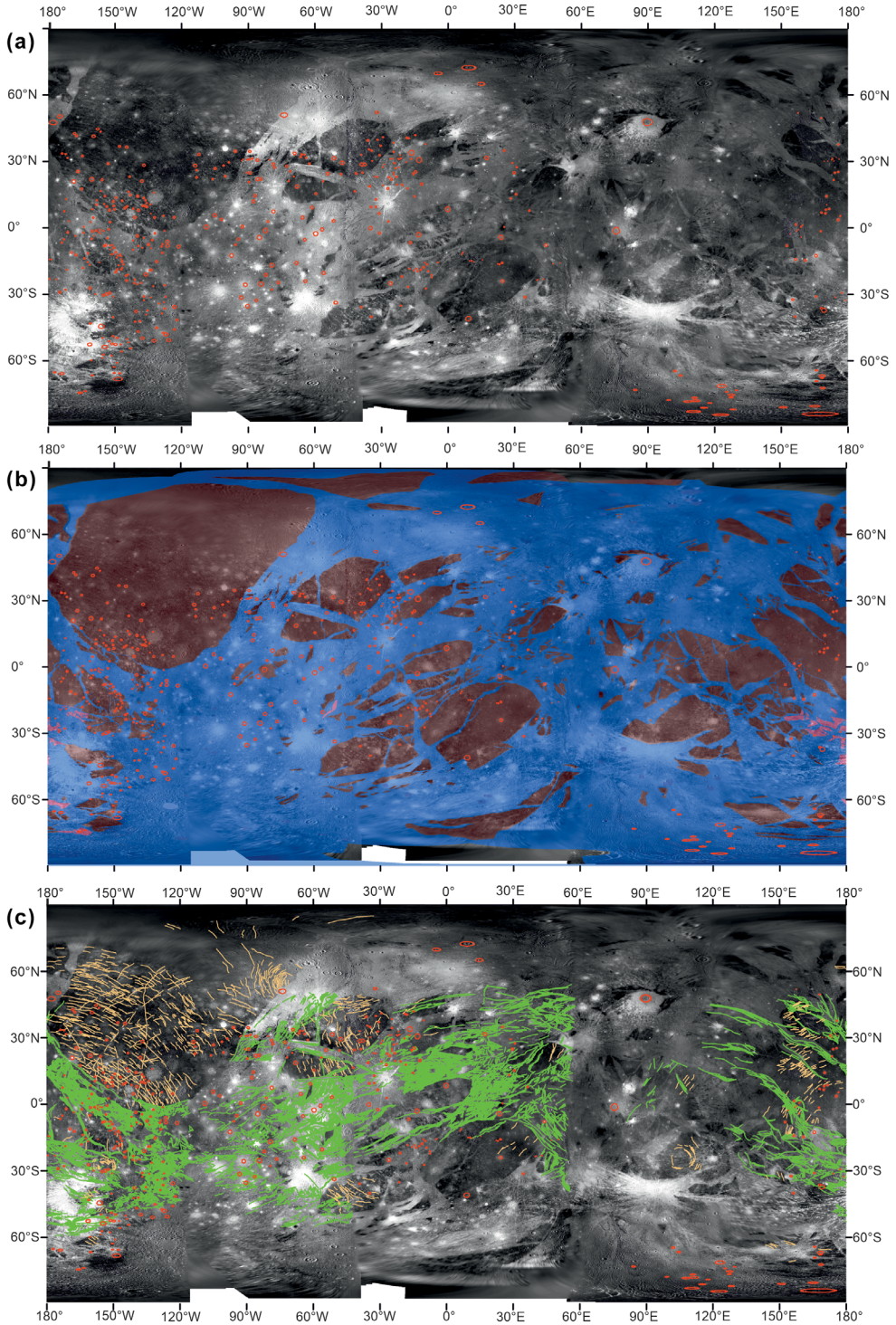

FIGURE 3. (a) Global base map of Ganymede in equidistant cylindrical projection (from Kersten et al., 2022) showing all mapped PICs (red). (b) The categorization of PICs based on the terrain type in which they are found: dark terrain (brown), light terrain (blue), and reticulate terrain (pink), according to the classification by Collins et al. (2013). (c) PICs in association with all the linear features (green and orange). The linear features on light terrain are mainly grooves (green, from Rossi et al., 2020), and the linear features on dark terrain are mainly furrows (orange, from Collins et al., 2013). (Color figure can be viewed at wileyonlinelibrary.com)

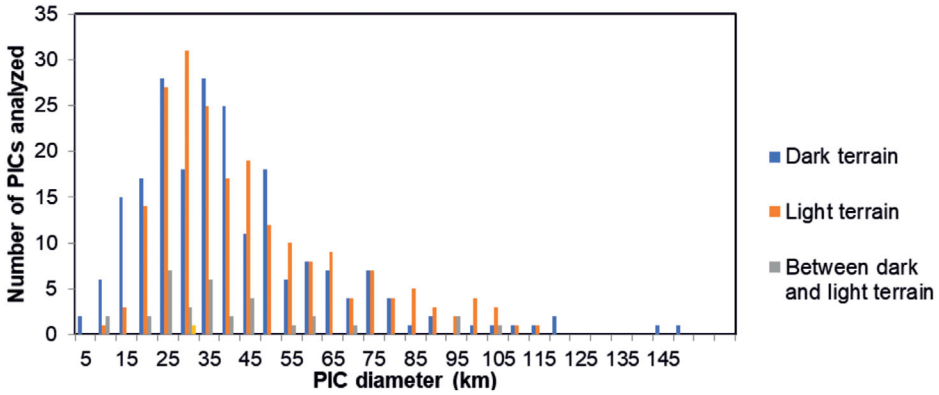

FIGURE 4. Histogram showing the diameter range of PICs in dark terrain, light terrain, reticulate terrain, and those located between dark terrain and light terrain. (Color figure can be viewed at wileyonlinelibrary.com)

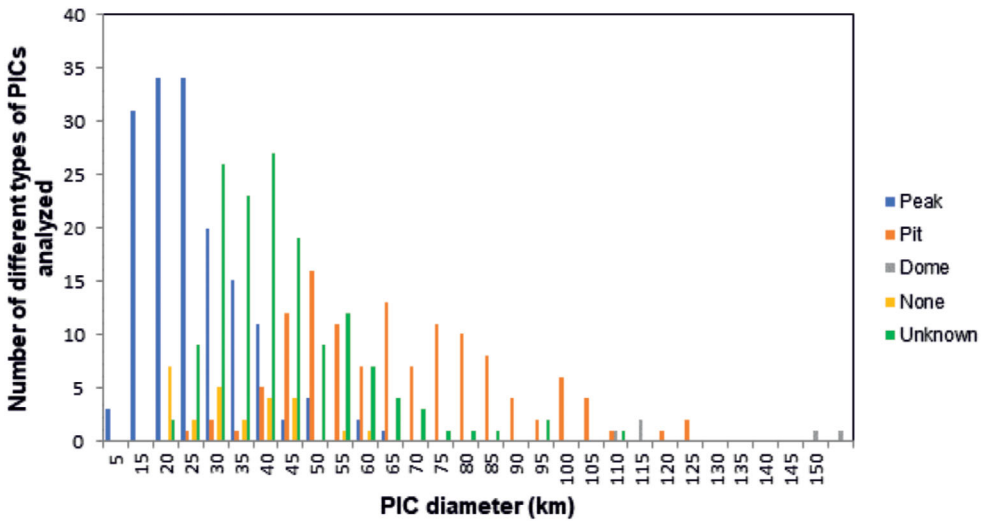

FIGURE 5. Histogram showing the distribution of different types of PICs across Ganymede. "None" is a category that lacks any central feature, and "unknown" represents a group of craters whose central feature could not be detected due to low resolution. (Color figure can be viewed at wileyonlinelibrary.com)

have a few straight segments that alternate with rounded sections of the perimeter.

Angularity

The deviation from a circular planform was quantified using an "Angularity" factor. For definition, we refer to the Methods section. Figure 7 shows the angularity values as a function of the diameter of PICs, subdivided for those identified as having peak, pit, dome, none, and unknown central features. The majority of the angularity values lie between 1.0 and 1.1, followed by values between 1.1 and 1.2, whereas 1.0 represents a circle. The density of points decreases from an angularity value of 1 toward an angularity value of 1.6. PICs that lie close to 1 still possess one or more straight segments, but

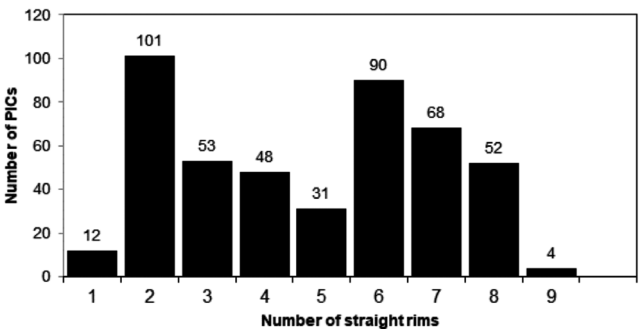

FIGURE 6. Histogram showing the number of straight segments possessed by different number of PICs.

the overall deviation from circularity is low. An angularity value close to 1.0 does not necessarily mean that a PIC has one or two straight segments. The highest

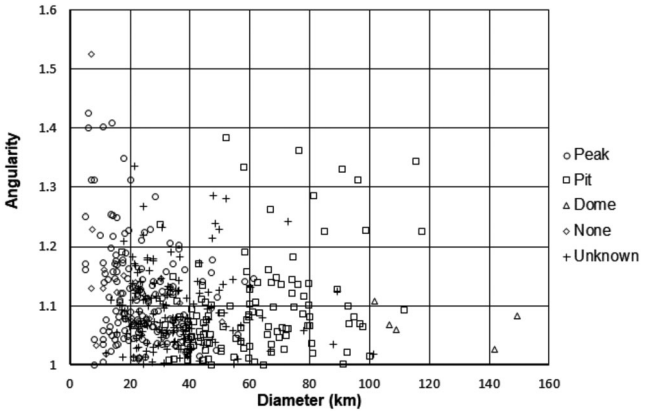

FIGURE 7. The graph displays the relationship between the diameter and angularity of the mapped PICs, whose central features are identified as peak, pit, dome, none, and unknown.

angularity values were observed for a few PICs with smaller diameters.

Linear Features and Influence on PICs

Since two thirds of Ganymede's surface are dominated by light terrain (Figure 3a; Pappalardo et al., 2004), which consists of ridges and grooves, the influence of these tectonic linear features on the morphology of the craters is obvious. However, as the density of PICs on dark terrain is apparently not less or even higher to that of the light terrain, the structurally controlling factors on dark terrain are likewise investigated. For this, we compare the major orientations of PICs straight segments and tectonic linear features of dark and light terrains from the sub-Jovian and the anti-Jovian hemispheres (Figure 8). We utilize the regional groove system map of light terrain (60°N–60°S) as presented by Rossi et al. (2020; Figure 3c). Similarly, to understand the structurally controlling factors on dark terrain, we utilize the global geological map as presented by Collins et al. (2013) in comparison to our mapped PICs.

In the light terrain, the grooves (Figure 3c) have a preferred orientation and are densely concentrated in regions of younger light terrain (Figure 3b). The dominant orientation of grooves from sub-Jovian and anti-Jovian hemispheres are in opposite directions: grooves in the sub-Jovian hemisphere have a dominant trend in the NE–SW direction, while grooves in the anti-Jovian hemisphere have a dominant trend in the NW–SE direction (Rossi et al., 2020). PICs are dominantly found in areas surrounding or within the grooved terrain. Particularly, from the available mapped global distribution of PICs, we find higher PIC density in regions within and around the Uruk sulcus region (Figure 3). This region is interpreted to be affected by transpressional strike-slip tectonics (Rossi et al., 2018). Figure 8 displays the orientation of a straight rim segments and the orientation of an adjacent linear feature. Data points that fall on the full diagonal line indicate that the orientation of a straight rim segment is parallel to that of nearby grooves. Data points that fall on the dashed diagonals indicate that the straight rim segment is perpendicular to nearby grooves. We found that most of the data points cluster around the diagonal, meaning that azimuths of rim segments are parallel with adjacent linear features for many of these PICs. In the case of PICs from light terrain of sub-Jovian hemisphere, we found 52% of straight rim segments aligned parallel with their adjacent linear features. For PICs from the light terrain of the anti-Jovian hemisphere, we found 65% of straight rim segments aligned parallel with their adjacent linear features.

In the dark terrain, the mapped furrows have a curvilinear appearance (Figure 3c) and are particularly frequent in the SW region of Galileo Regio, the largest coherent dark terrain. The dominant orientation of furrows from the sub-Jovian and anti-Jovian hemispheres are NW–SE directions. The dark terrain area with the highest number of PICs is located in Galileo Regio, adjacent to Uruk Sulcus (Figure 3). The different types of dark terrain and the major and minor tectonic activities affecting the formation of furrows and fractures on dark terrain are listed in Table 1. In the case of PICs from the dark terrain of the sub-Jovian hemisphere, we found that 71% of straight rim segments aligned parallel with their adjacent linear features. For PICs from the dark terrain of the anti-Jovian hemisphere, only 39% of straight rim segments aligned parallel with their adjacent linear features.

To conclude, the orientation analyses of straight rim segments and adjacent grooves show that the latter indeed govern the orientation of straight crater rims. Lineaments and grooves are, first of all, surface features of unknown origin. If they would just sculpture the surface, they would cause no effect on crater formation. However, the fact that they indeed lead to a localization of deformation and constrain the position of the crater rim segments during the cratering process gives independent proof that the surface features go deep into the icy crust. The observation is proof that the lineations and grooves represent fault scarps and traces of faults. The faults have damaged the crust and thus created planar zones of mechanical weakness. The similar number of PICs on dark and light terrain indicates that both types of terrains behave mechanically similar and contain such faults. However, in Galileo Regio, Perrine Regio, Melotte Regio, and Marius Regio, the major cause for linear features are identified to be furrows from ancient large impact event. In the Nicholson Regio, the linear features are due to

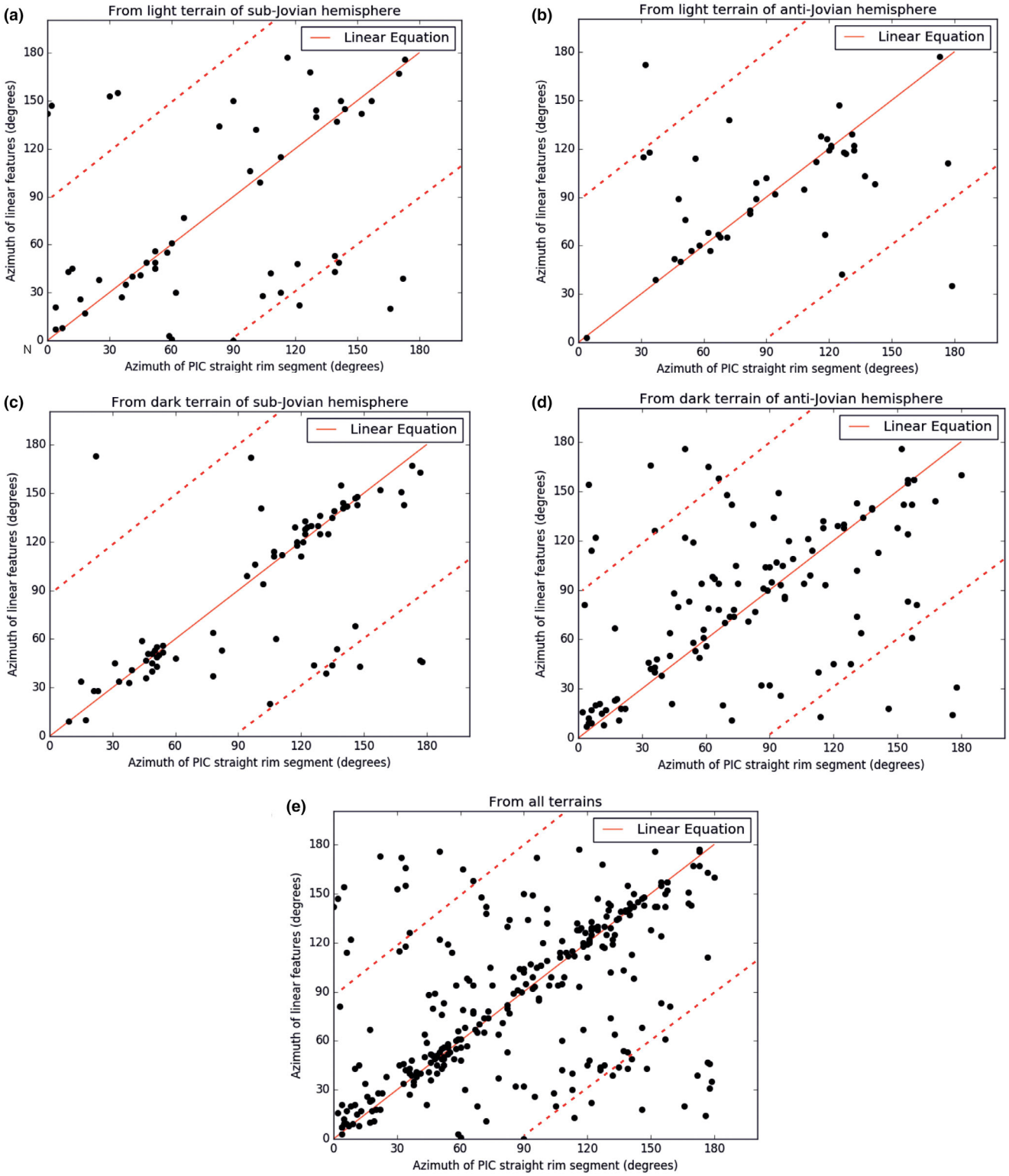

FIGURE 8. Azimuth comparisons of straight rim segments of PICs and adjacent tectonic linear features. (a) From the light terrain of the sub-Jovian hemisphere; (b) from the light terrain of the anti-Jovian hemisphere; (c) from the dark terrain of the sub-Jovian hemisphere; (d) from the dark terrain of the anti-Jovian hemisphere; (e) combined analysis from all terrains. Note that the solid red line represents a regression line illustrating similar azimuths. The red dashed lines illustrate perpendicular azimuths. (Color figure can be viewed at wileyonlinelibrary.com)

TABLE 1. The different types of dark terrains and the number of PICs mapped from them are noted. The major and minor form of linear features responsible for determining the polygonal shape for the craters emplaced on dark terrains are also listed. In cells that are blank, we indicate that we do not observe any linear features.

	Dark terrain	Number of PICs observed	Main linear features influencing PICs	Cause for main linear features	Minor linear features influencing PICs	Cause for minor linear features
1	Galileo Regio	139	Lakhmu furrow	Old impact (Schenk & McKinnon, 1987; Zuber & Parmentier, 1984)	Zu fossae	Strike-slip faulting (Rossi et al., 2023)
2	Perrine Regio	33	NW–SE furrows	Large impact	E–W trending furrow	Impact related
3	Barnard Regio	2	NW–SE furrows	Large impact	—	—
4	Nicholson Regio	30	NW–SE linear features	Dark lineated terrain formation	NE–SW linear features	Probably related to the impact of Enkidu crater
5	Melotte Regio	2	Concentric fractures	Old impact	Unknown (low resolution)	Unknown (low resolution)
6	Marius Regio	29	NE–SW linear features	Old impact (Schenk & McKinnon, 1987; Zuber & Parmentier, 1984)	—	—

the development of dark lineated terrain formed via tectonic resurfacing activities (Table 1).

PICs in Galileo Regio

Galileo Regio, the largest of the dark terrain, mostly shows concentric furrows (Figure 9a). The age of dark terrains like Galileo Regio, in general, is estimated to be ~4 Gyr, which represents one of the oldest terrains on Ganymede (Baby et al., 2023; Neukum, 1997; Zahnle et al., 2003). The number of PICs in Galileo Regio is the largest of all dark terrain, and the density of PICs per area (Figures 3b and 9a) seems to positively correlate with the number of furrows, although this is only a qualitative statement. The PICs in Galileo Regio have well-developed straight rim segments.

PICs are influenced by the furrows of Lakhmu and Zu fossae but are also found within or between furrows. There is a higher number of furrows related to Lakhmu fossae than to Zu fossae. Both of them seem to control the abundance of PICs. The mapped PICs postdate furrow formation. Here, straight rim segments of PICs are commonly found to have irregular hexagonal to octagonal shapes (Figure 9b). The rose diagram of straight rim segments of PICs (Figure 9c) shows various orientations and a subdued concentration of WNW–ESE and NE–SW directions. While the rose diagram of the furrows (Figure 9d) has a clear preferred orientation in the NW–SE direction. The discrepancy between furrow orientation and straight rim orientation is less obvious, but this might be an artifact due to the concentric character of the furrows.

DISCUSSION

Formation Mechanism of PICs on Ganymede

Our analysis revealed that the majority of azimuths of straight rim segments align parallel or subparallel to adjacent tectonic linear features (Figure 8). This observation leads us to infer that the development of polygonal shapes is primarily influenced by deep-rooted faults that represent planes of crustal weaknesses and got reactivated during crater formation. However, we also observed non-parallel or perpendicular relationships between straight rim segments and their adjacent tectonic linear features in some cases, suggesting that these particular straight rim segments might result from surface expressions rather than deep-rooted faults. In addition, ice is known as one of the mechanically most anisotropic crystals (e.g., Duval et al., 2010). If the icy crust of Ganymede has experienced some shearing or flow, a crystallographic preferred orientation may form, which may result in large-scale crustal anisotropies that can also affect the crater-forming process.

The dominantly parallel alignment of straight segments of PICs with furrows, grooves, and lineaments suggest at the formation mechanism of PICs' straight rim segments occurred during the modification stage of cratering. The additional presence of straight rims perpendicular to the lineation orientation (Figure 8) is somewhat surprising. For instance, for individual PICs in Galileo Regio, there are at least two straight rim segments within each PICs that are parallel and at perpendicular angles with respect to the furrows. When the crater is

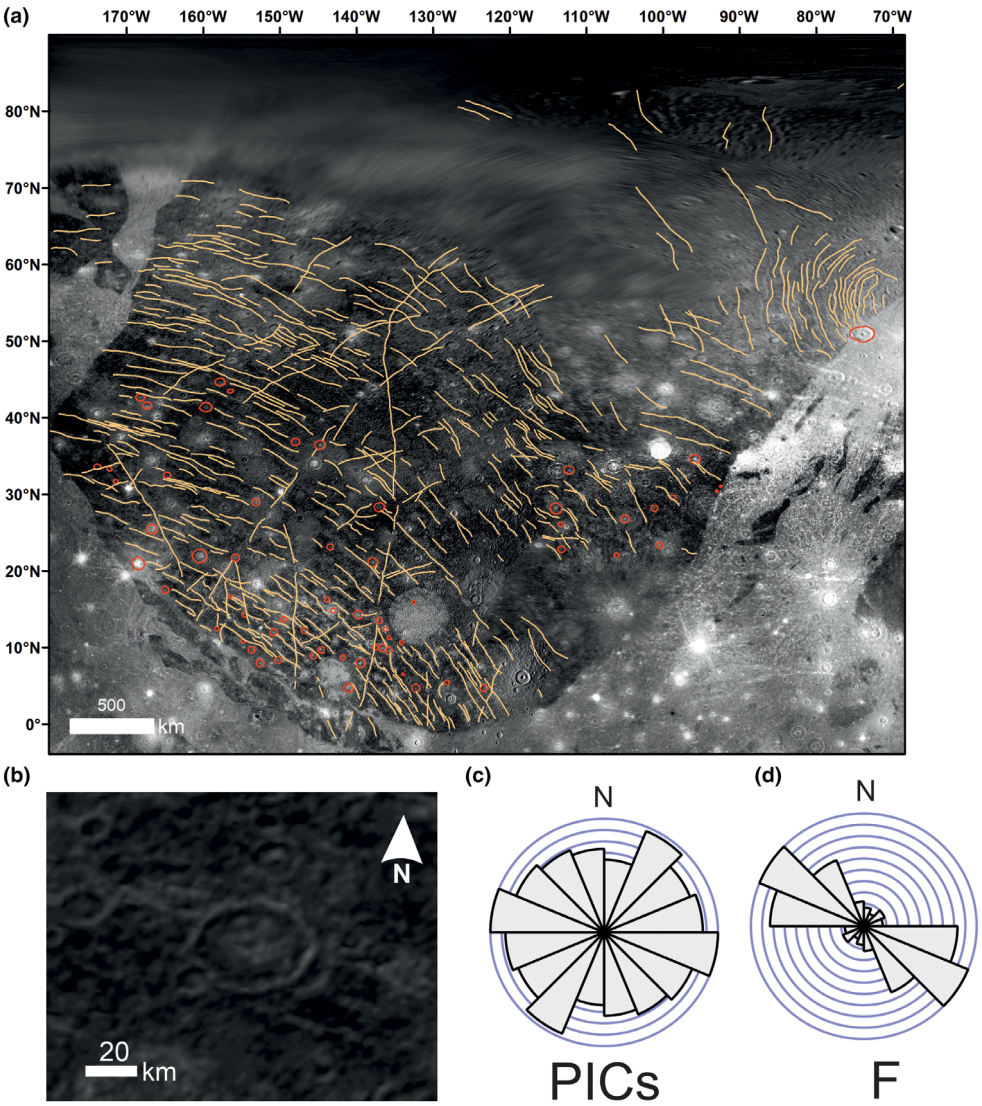

FIGURE 9. (a) Distribution of PICs and lineaments on Galileo Regio. Note that PICs are indicated by red circles and furrows by orange lines (from Collins et al., 2013). (b) Close-up view of a hexagonal-shaped PIC in Galileo Regio. (c) Rose diagram showing the orientation of straight rim segments of all PICs. (d) Rose diagram showing the orientation of all furrows. (Color figure can be viewed at wileyonlinelibrary.com)

emplaced on densely and differently oriented linear features, then the resulting PIC would have the tendency to obtain a greater number of straight segments, which, in distant view, appear more toward circular shape. Thus, the presence of one fault and one straight segment may govern the entire crater collapse process and induce additional straight segments, although they are probably not supported by an anisotropic target strength.

On Ganymede, the spatial resolution did not allow to investigate simple craters and their potential polygonality. The simple-to-complex transition diameter on Ganymede is ~5 km (Schenk, 1991). Similarly, the transition diameters from the central peak to the central pit crater are inversely proportional to surface gravity. The formation of polygonal crater outlines seems not to be affected by these different crater types. The surface temperatures on Ganymede, down to ~100 K, cause ice that is stronger than the ice on terrestrial planets, but still, the static tensile and compressive strength are lower than those of rocks (Durham & Stern, 2001). So Ganymede's icy crust is sufficiently brittle to allow the formation and also the preservation of distinct polygonal shapes. Relaxation affects the crater floor and can induce alterations to the crater rim (Singer et al., 2018). Viscous relaxation is wavelength dependent and progresses more rapidly for larger craters, potentially reducing their depths, while it has a lesser effect on smaller craters (Bland et al., 2017; Singer et al., 2018). Numerous craters on Ganymede

exhibit some degree of relaxation, primarily attributed to radiogenic heat flow (Bland et al., 2017).

Comparison to Ceres and Dione

A comparison of Ganymede with the dwarf planet Ceres of the asteroid belt and the moon of Saturn, Dione, is presented here to assess the influence of linear features, crustal composition temperature, and gravity in governing the development of PIC formation. In terms of distance from the Sun and surface temperature, Ganymede is located between Ceres and Dione.

Ceres has much warmer ice than Ganymede and Dione. The near-subsurface temperature is estimated to range from about 180 K at the equator to approximately 130 K at the poles (Fanale & Salvail, 1989). The acceleration due to gravity is $\sim 0.28\ m\ s^{-2}$ (similar to Dione). On Ceres, linear tectonic features in the form of furrows, ridges, troughs, and scarps are widely spaced across the surface (Buczkowski et al., 2016). The lower number of linear tectonic features is ascribed to the resurfacing in the form of impacts playing a dominant role (Hiesinger et al., 2016). About 3% of impact craters on Ceres are identified to represent PICs (Zeilnhofer & Barlow, 2021). Most of these PICs are found adjacent to tectonic linear features and the other PICs, which suggests extensive subsurface fracturing (Zeilnhofer & Barlow, 2021).

Dione's surface temperature exhibits a lower average compared to celestial bodies such as Ceres and Ganymede. The thermal variations on Dione, ranging from equatorial to polar regions, span an approximate range of 50–90 K (Howett et al., 2010). The acceleration due to gravity is $0.232\ m\ s^{-2}$. On Dione, the surface is heavily cratered, but in areas like the wispy terrain (found mostly in trailing hemisphere), it contains faults (Smith et al., 1981, 1982). The non-wispy region, which was previously thought to be only cratered does also possess sub-surface fractures due to the presence of PICs found (Beddingfield et al., 2016). 35% of impact craters of non-wispy terrain are inferred to be PICs (Beddingfield et al., 2016).

Unlike Ganymede, Ceres and Dione surfaces are densely cratered, and visible tectonic linear features are concentrated in a few areas globally. However, non-visible linear features due to subsurface fracturing are reported for Ceres (Otto et al., 2016; Zeilnhofer & Barlow, 2021) and Dione (Beddingfield et al., 2016) based on the presence of PICs. On Ganymede faults and fractures-forming grooves and lineations are widespread and visible, and there seems to be a correlation of their frequency with the number of PICs. Ganymede's crustal temperature is intermediate between that of Ceres and Dione. The acceleration due to gravity of Ganymede is $1.428\ m\ s^{-2}$. Gravity affects the fault scaling relationship of fault length to fault displacement and fault width (Schultz et al., 2006). Thus, for a given fault length, the displacement and width are less on a low-gravity body. This circumstance may influence the amount of strength degradation due to faulting.

On Ganymede, we found that all of the mapped PICs are situated near at least one tectonic linear feature. Faults and fractures are not restricted to the light terrain but are also frequent on the dark terrain. Thus, in contrast to Ceres and Dione, faults causing polygonality are surface ruptures. The surface temperatures of Ganymede and Dione are down to ~100 K (Durham & Stern, 2001), suggesting that their crusts behave more brittle than that of Ceres. On the Ceres fault, obliteration by thermal relaxation and surface degradation seems to be more active.

We do not know the exact ages of these three icy bodies, nor whether they accreted from their present location or were captured into their current resonance (e.g., Showman et al., 1997; Sinclair, 1972). Also, we are not certain of the specific combination of processes, such as global volume expansion, Laplace resonance, orbital recession, non-synchronous rotation, and large impacts, that are responsible for initiating tectonic activity on these bodies. However, based on the present-day scenario, Ganymede exhibits less cratering and more pronounced tectonic activity compared to Ceres and Dione, as evidenced by the densely distributed and globally pervasive tectonic linear features on its surface.

CONCLUSIONS

This study is the first report and analysis of PICs on Ganymede,

- PICs occur on both the light and dark terrain. The high number of PICs on dark terrain partly results from the being more densely cratered.
- All of the mapped PICs are complex craters and have either a peak, a pit, or a dome as central morphological feature. The PICs attain their final polygonal shape during the modification stage via slumping/ faulting along preexisting fractures and fault planes of weakness.
- Among impact craters of 30 km and larger, PICs constitute 30% of the crater population present on Ganymede. This is consistent with the results of PICs from other icy bodies.
- The comparative analysis of the orientation of PICs straight rim segments and adjacent linear features indicates that there exists a genetic relationship between PICs and linear features. This implies that linear features are not only surface markers but also act as mechanical anisotropies and zone of crustal

weakness. This study provides independent proof that grooves and lineations are the traces of faults.
- PICs on Ganymede postdate tectonic activities in the light and dark terrain.
- The abundance of PICs on a planetary body relative to the entire crater population is a measure of the mechanical anisotropy of the particular crust and seems to correlate with the intensity of the tectonic activity of that body.
- Ganymede's icy crust is sufficiently brittle to allow the formation and preservation of distinct polygonal shapes. Relaxation affects the crater floor of many craters but does not degrade their rims. This suggests that relaxation is caused by localized impact-induced thermal anomalies in the crater centers.

Acknowledgments—We gratefully acknowledge the DLR-DAAD PhD fellowship from the German Aerospace Center and the German Academic Exchange Service. Special thanks to Costanza Rossi for sharing Ganymede's regional groove system data. We thank the editor and two anonymous reviewers for their detailed comments and suggestions, which greatly contributed to the improvement of this manuscript. Open Access funding enabled and organized by Projekt DEAL.

Conflict of Interest Statement—We declare no conflict of interest.

Data Availability Statement—Data available on request.

Editorial Handling—Dr. Jeffrey Plescia

REFERENCES

Abels, A. 2003. Investigation of Impact Structures in Finland (Söderfjärden, Lumparn, Lappajärvi) by Digital Integration of Multidisciplinary Geodata. Inaugural Dissertation for Attaining the Doctoral Degree in Natural Sciences, Westfalian-Wilhelms University, Mü finster, Germany (CD-ROM).

Aittola, M., Öhman, T., Leitner, J. J., Kostama, V. P., and Raitala, J. 2010. The Structural Control of Venusian Polygonal Impact Craters. *Icarus* 205: 356–363.

Anderson, J. L., Schultz, P. H., and Heineck, J. T. 2003. Asymmetry of Ejecta Flow during Oblique Impacts Using Three-Dimensional Particle Image Velocimetry. *Journal of Geophysical Research: Planets* 108(E8): 5094. https://doi.org/10.1029/2003je002075.

Aschauer, J., and Kenkmann, T. 2017. Impact Cratering on Slopes. *Icarus* 290: 89–95.

Baby, N. R., Wagner, R. J., Stephan, K., and Kenkmann, T. 2023. Stratigraphy, Crater Size–Frequency Distribution, and Chronology of Selected Areas of Ganymede's Light and Dark Terrains. *The Planetary Science Journal* 4: 162. https://doi.org/10.3847/PSJ/acebed.

Beddingfield, C. B., Beyer, R., Cartwright, R. J., Singer, K., Robbins, S., Stern, S. A., Bray, V., et al. 2020. Polygonal Impact Craters on Charon Lunar and Planetary Science Conference, abstract #2326, p. 1241.

Beddingfield, C. B., Burr, D. M., and Tran, L. T. 2016. Polygonal Impact Craters on Dione: Evidence for Tectonic Structures outside the Wispy Terrain. *Icarus* 274: 163–194.

Beddingfield, C. B., and Cartwright, R. J. 2020. Hidden Tectonism on Miranda's Elsinore Corona Revealed by Polygonal Impact Craters. *Icarus* 343: 113687.

Beddingfield, C. B., Cartwright, R. J., Patthoff, D. A., Beyer, R., and Moore, J. 2022. Investigating Hidden Fractures on Iapetus Using Polygonal Impact Craters. *LPI Contributions* 2678: 1077.

Bland, M. T., Singer, K. N., McKinnon, W. B., and Schenk, P. M. 2017. Viscous Relaxation of Ganymede's Impact Craters: Constraints on Heat Flux. *Icarus* 296: 275–288.

Boyce, J., Barlow, N., Mouginis-Mark, P., and Stewart, S. 2010. Rampart Craters on Ganymede: Their Implications for Fluidized Ejecta Emplacement. *Meteoritics & Planetary Science* 45: 638–661.

Buczkowski, D. L., Schmidt, B. E., Williams, D. A., Mest, S. C., Scully, J. E. C., Ermakov, A. I., et al. 2016. The Geomorphology of Ceres. *Science* 353: aaf4332.

Collins, G. 2000. Driving Mechanisms for Grooved Terrain Tectonics on Ganymede and Chaotic Terrain Fonnation on Europa: Constraints from Galileo Data. PhD thesis, Brown University.

Collins, G. C., Head, J. W., and Pappalardo, R. T. 1998. Formation of Ganymede Grooved Terrain by Sequential Extensional Episodes: Implications of Galileo Observations for Regional Stratigraphy. *Icarus* 135: 345–359.

Collins, G. C., Patterson, G. W., Head, J. W., Prockter, L., Pappalardo, R. T., Lucchitta, B. K., and Kay, J. P. 2013. Global Geologic Map of Ganymede, p. 3237 US Department of the Interior, US Geological Survey.

Crow-Willard, E. N., and Pappalardo, R. T. 2015. Structural Mapping of Enceladus and Implications for Formation of Tectonized Regions. *Journal of Geophysical Research: Planets* 120: 928–950.

Darling, J. A., and Mes, A. 1948. Crater Tests in Basalt. Department of Operations and Maintenance, Spec, Engineering Dium, Panama Canal Zone, ICS Memo.

Dasgupta, D., Kundu, A., De, K., and Dasgupta, N. 2019. Polygonal Impact Craters in the Thaumasia Minor, Mars: Role of Pre-Existing Faults in their Formation. *Journal of the Indian Society of Remote Sensing* 47: 257–265.

De Sanctis, M. C., Ammannito, E., Raponi, A., Marchi, S., McCord, T. B., McSween, H. Y., Capaccioni, F., et al. 2015. Ammoniated Phyllosilicates with a Likely Outer Solar System Origin on (1) Ceres. *Nature* 528: 241–44.

Denk, T., Neukum, G., Helfenstein, P., Thomas, P. C., Turtle, E. P., McEwen, A. S., et al. 2005. The First Six Month of Iapetus Observations by the Cassini ISS Camera. *36th Lunar and Planetary Science*, abstract #2262, p. 1734.

Durham, W. B., and Stern, L. A. 2001. Rheological Properties of Water Ice—Applications to Satellites of the Outer Planets. *Annual Review of Earth and Planetary Sciences* 29: 295–330.

Duval, P., Montagnat, M., Grennerat, F., Weiss, J., Meyssonnier, J., and Philip, A. 2010. Creep and Plasticity of Glacier Ice: A Material Science Perspective. *Journal of Glaciology* 56: 1059–68.

Eppler, D. T., Ehrlich, R., Nummedal, D., and Schultz, P. H. 1983. Sources of Shape Variation in Lunar Impact Craters: Fourier Shape Analysis. *Geological Society of America Bulletin* 94: 274–291. https://doi.org/10.1130/0016-7606(1983)94274:SOSVIL2.0.CO;2.

Fanale, F. P., and Salvail, J. R. 1989. The Water Regime of Asteroid (1) Ceres. *Icarus* 82: 97–110.

Ferguson, S. N., Rhoden, A. R., and Kirchoff, M. R. 2020. Small Impact Crater Populations on Saturn's Moon Tethys and Implications for Source Impactors in the System. *Journal of Geophysical Research: Planets* 125: e2020JE006400.

Figueredo, P. H., and Greeley, R. 2004. Resurfacing History of Europa from Pole-to-Pole Geological Mapping. *Icarus* 167: 287–312.

Gault, D. E., Quaide, W. L., and Oberbeck, V. R. 1968. Impact Cratering Mechanics and Structures. In *Shock Metamorphism of Natural Materials*, edited by B. M. French, and N. M. Short, 87–99. Mono Book Corporation, Baltimore, MD.

Gottwald, M., Kenkmann, T., and Reimold, W. U. 2020. *Terrestrial Impact Structures: The TanDEM-X Atlas*. München: Verlag Dr Friedrich Pfeil. 608.

Greeley, R., Klemaszewski, J. E., and Wagner, R. 2000. Galileo Views of the Geology of Callisto. *Planetary and Space Science* 48: 829–853.

Hansen, C. J., Bolton, S., Sulaiman, A. H., Duling, S., Bagenal, F., Brennan, M., et al. 2022. Juno's Close Encounter with Ganymede—An Overview. *Geophysical Research Letters* 49: e2022GL099285.

Hartman, W. K. 1980. Surface Evolution of Two-Component Stone/Ice Bodies in the Jupiter Region. *Icarus* 44: 441–453.

Hibbitts, C. A., Pappalardo, R. T., Hansen, G. B., and McCord, T. B. 2003. Carbon Dioxide on Ganymede. *Journal of Geophysical Research: Planets* 108(E5): 5036. https://doi.org/10.1029/2002JE001956.

Hiesinger, H., Marchi, S., Schmedemann, N., Schenk, P., Pasckert, J. H., Neesemann, A., O'Brien, D. P., et al. 2016. Cratering on Ceres: Implications for its Crust and Evolution. *Science* 353: aaf4759.

Hirata, N., Suetsugu, R., and Ohtsuki, K. 2020. A Global System of Furrows on Ganymede Indicative of their Creation in a Single Impact Event. *Icarus* 352: 113941.

Howett, C. J. A., Spencer, J. R., Pearl, J., and Segura, M. 2010. Thermal Inertia and Bolometric Bond Albedo Values for Mimas, Enceladus, Tethys, Dione, Rhea and Iapetus as Derived from Cassini/CIRS Measurements. *Icarus* 206: 573–593.

Johnson, R. B. 1962. Effect of Geologic Factors on Cratering Experiments in Basalt, Buckboard Mesa, Nevada Test Site, Nevada. US Department of the Interior, Geological Survey.

Jones, K. B., Head, J. W., III, Pappalardo, R. T., and Moore, J. M. 2003. Morphology and Origin of Palimpsests on Ganymede Based on Galileo Observations. *Icarus* 164: 197–212.

Kenkmann, T. 2021. The Terrestrial Impact Crater Record: A Statistical Analysis of Morphologies, Structures, Ages, Lithologies, and More. *Meteoritics & Planetary Science* 56: 1024–70. https://doi.org/10.1111/maps.13657.

Kersten, E., Zubarev, A. E., Nadezhdina, I. E., Roatsch, T., Matz, K.-D., and Szczech, C. C. 2022EPSC2022-450, Granada, Spain. September 18–23. Updated Ganymede Mosaic from Juno Perijove 34 Images, Europlanet Science Congress https://doi.org/10.5194/epsc2022-450.

Kersten, E., Zubarev, A. E., Roatsch, T., and Matz, K. D. 2021. Controlled Global Ganymede Mosaic from Voyager and Galileo Images. *Planetary and Space Science* 206: 105310.

Kumar, P. S., and Kring, D. A. 2008. Impact Fracturing and Structural Modification of Sedimentary Rocks at Meteor Crater, Arizona. *Journal of Geophysical Research: Planets* 113: E09009. https://doi.org/10.1029/2008JE003115.

Melosh, H. J. 1989. *Impact Cratering: A Geologic Process*. New York/Oxford: Oxford University Press/Clarendon Press.

Moore, J. M. 1984. The Tectonic and Volcanic History of Dione. *Icarus* 59: 205–220.

Moore, J. M., Horner, V. M., and Greeley, R. 1985. The Geomorphology of Rhea: Implications for Geologic History and Surface Processes. *Journal of Geophysical Research* 90(S02): C785. https://doi.org/10.1029/jb090is02p0c785.

Neidhart, T., Leitner, J. J., and Firneis, M. G. 2017. Polygonal Impact Craters on Rhea, Dione, Tethys, Ceres, and Vesta. *48th Annual Lunar and Planetary Science Conference*, abstract #1964, p. 1625.

Neukum, G. 1997. Bombardment History of the Jovian System. In *The Three Galileos: The Man, the Spacecraft, the Telescope*, 201–212. Dordrecht: Springer.

Öhman, T., Aittola, M., Korteniemi, J., Kostama, V. P., and Raitala, J. 2010. Polygonal Impact Craters in the Solar System: Observations and Implications.

Öhman, T., Aittola, M., Kostama, V. P., Raitala, J., and Korteniemi, J. 2008. Polygonal Impact Craters in Argyre Region, Mars: Implications for Geology and Cratering Mechanics. *Meteoritics & Planetary Science* 43: 1605–28.

Öpik, E. J. 1969. The Moon's Surface. *Annual Review of Astronomy and Astrophysics* 7: 473–526.

Otto, K. A., Jaumann, R., Krohn, K., Buczkowski, D., von der Gathen, I., Kersten, E., Russell, C. T., and Mest, S. C. 2016. Polygonal Impact Craters on Ceres: Morphology and Distribution. 79th Annual Meeting of the Meteoritical Society, 6460 p.

Pappalardo, R. T., Collins, G. C., Head, J. W., Helfenstein, P., McCord, T. B., Moore, J. M., Prockter, L. M., et al. 2004. Geology of Ganymede. In *Jupiter*, edited by F. D. Bagenal, T. E. Dowling, and W. B. McKinnon, 363–396. Cambridge, UK: Cambridge University Press.

Patterson, G. W., Collins, G. C., Head, J. W., Pappalardo, R. T., Prockter, L. M., Lucchitta, B. K., and Kay, J. P. 2010. Global Geological Mapping of Ganymede. *Icarus* 207: 845–867.

Pierazzo, E., and Collins, G. 2004. A Brief Introduction to Hydrocode Modeling of Impact Cratering. In *Cratering in Marine Environments and on Ice*, edited by H. Dypvik, M. J. Burchell, and P. Claeys, 323–340. Berlin, Heidelberg: Springer. https://doi.org/10.1007/978-3-662-06423-8_16.

Plescia, J. B. 1987. Geological Terrains and Crater Frequencies on Ariel. *Nature* 327: 201–4. https://doi.org/10.1038/327201a0.

Poelchau, M. H., Kenkmann, T., and Kring, D. A. 2009. Rim Uplift and Crater Shape in Meteor Crater: Effects of Target Heterogeneities and Trajectory Obliquity. *Journal of Geophysical Research: Planets* 114(E1): E01006. https://doi.org/10.1029/2008JE003235.

Porco, C. C., Baker, E., Barbara, J., Beurle, K., Brahic, A., Burns, J. A., et al. 2005. Cassini Imaging Science: Initial Results on Phoebe and Iapetus. *Science* 307: 1237–42.
Prettyman, T. H., Yamashita, N., Toplis, M. J., McSween, H. Y., Schörghofer, N., Marchi, S., Feldman, W. C., et al. 2017. Extensive Water Ice within Ceres' Aqueously Altered Regolith: Evidence from Nuclear Spectroscopy. *Science* 355: 55–59. https://doi.org/10.1126/science.aah6765.
Ravine, M. A., Hansen, C. J., Collins, G. C., Schenk, P. M., Caplinger, M. A., Lipkaman Vittling, L., et al. 2022. Ganymede Observations by JunoCam on Juno Perijove 34. *Geophysical Research Letters* 49: e2022GL099211.
Rossi, C., Cianfarra, P., and Salvini, F. 2020. Structural Geology of Ganymede Regional Groove Systems (60°N–60°S). *Journal of Maps* 16: 6–16.
Rossi, C., Cianfarra, P., Salvini, F., Mitri, G., and Massé, M. 2018. Evidence of Transpressional Tectonics on the Uruk Sulcus Region, Ganymede. *Tectonophysics* 749: 72–87.
Rossi, C., Lucchetti, A., Massironi, M., Penasa, L., Pozzobon, R., Munaretto, G., and Pajola, M. 2023. Multi-Phase Activity on Ganymede's Dark Terrain: Tectonic Evolution of Galileo Regio. *Icarus* 390: 115305.
Schenk, P. M. 1991. Ganymede and Callisto: Complex Crater Formation and Planetary Crusts. *Journal of Geophysical Research: Planets* 96: 15635–64.
Schenk, P. M., and McKinnon, W. B. 1987. Ring Geometry on Ganymede and Callisto. *Icarus* 72: 209–234.
Schenk, P. M., McKinnon, W. B., Gwynn, D., and Moore, J. M. 2001. Flooding of Ganymede's Bright Terrains by Low-Viscosity Water-Ice Lavas. *Nature* 410: 57–60.
Schultz, P. H. 1976. *Moon Morphology: Interpretations Based on Lunar Orbiter Photography*. Austin, TX: University of Texas Press.
Schultz, R. A., Okubo, C. H., and Wilkins, S. J. 2006. Displacement-Length Scaling Relations for Faults on the Terrestrial Planets. *Journal of Structural Geology* 28: 2182–93.
Shoemaker, E. M. 1963. Impact Mechanics at Meteor Crater, Arizona. In *The Moon, Meteorites and Comets. The Solar System, IV*, edited by B. M. Middlehurst, and G. P. Kuiper, 301–336. Chicago, IL: University of Chicago Press.
Shoemaker, E. M., Lucchitta, B. K., Wilhelms, D. E., Plescia, J. B., and Squyres, S. W. 1982. The Geology of Ganymede. In *Satellites of Jupiter*, edited by D. Morrison, 435–520. Tucson, AZ: University of Arizona Press.
Showman, A. P., Stevenson, D. J., and Malhotra, R. 1997. Coupled Orbital and Thermal Evolution of Ganymede. *Icarus* 129: 367–383.
Sinclair, A. T. 1972. On the Origin of the Commensurabilities amongst the Satellites of Saturn. *Monthly Notices of the Royal Astronomical Society* 160: 169–187.
Singer, K. N., Bland, M. T., Schenk, P. M., and McKinnon, W. B. 2018. Relaxed Impact Craters on Ganymede: Regional Variation and High Heat Flows. *Icarus* 306: 214–224. https://doi.org/10.1016/j.icarus.2018.01.012.
Singer, K. N., and McKinnon, W. B. 2011. Tectonics on Iapetus: Despinning, Respinning, or Something Completely Different? *Icarus* 216: 198–211.
Smith, B. A., Soderblom, L., Batson, R., Bridges, P., Inge, J., Masursky, H., Shoemaker, E., et al. 1982. A New Look at the Saturn System: The Voyager 2 Images. *Science* 215: 504–537.
Smith, B. A., Soderblom, L., Beebe, R., Boyce, J., Briggs, G., Bunker, A., Collins, S. A., et al. 1981. Encounter with Saturn: Voyager 1 Imaging Science Results. *Science* 212: 163–191.
Soderblom, J. M., Brown, R. H., Soderblom, L. A., Barnes, J. W., Jaumann, R., Le Mouélic, S., et al. 2010. Geology of the Selk Crater Region on Titan from Cassini VIMS Observations. *Icarus* 208: 905–912.
Stephan, K., Jaumann, R., Zambon, F., Carrozzo, F. G., Wagner, R., Longobardo, A., Palomba, E., et al. 2019. Ceres' Impact Craters—Relationships between Surface Composition and Geology. *Icarus* 318: 56–74.
Stephan, K., Roatsch, T., Tosi, F., Matz, K. D., Kersten, E., Wagner, R., et al. 2021. Regions of Interest on Ganymede's and Callisto's Surfaces as Potential Targets for ESA's JUICE Mission. *Planetary and Space Science* 208: 105324.
Talvitie, J., Pernu, T., and Raitala, J. 1975. *The Circular Vaasastructure in the Baltic Shield, Western Finland*.Contribution# 59. Finland: Department of Geophysics, University of Oulu. 15.
Watters, W. A., Grotzinger, J. P., Bell, J., Grant, J., Hayes, A. G., Li, R., Squyres, S. W., et al. 2011. Origin of the Structure and Planform of Small Impact Craters in Fractured Targets: Endurance Crater at Meridiani Planum, Mars. *Icarus* 211: 472–497. https://doi.org/10.1016/j.icarus.2010.08.030.
Weber, P., Zeilnhofer, M. F., Martorana, M., and Nocera, K. 2022. Regional Investigations of Polygonal Impact Craters on the Moon and Vesta. *Research Notes of the AAS* 6: 87.
Weihs, G. T., Leitner, J. J., and Firneis, M. G. 2015. Polygonal Impact Craters on Mercury. *Planetary and Space Science* 111: 77–82.
Zahnle, K., Schenk, P., Levison, H., and Dones, L. 2003. Cratering Rates in the Outer Solar System. *Icarus* 163: 263–289.
Zeilnhofer, M. F., and Barlow, N. G. 2021. The Characterization and Distribution of Polygonal Impact Craters on Ceres and their Implications for the Cerean Crust. *Icarus* 368: 114586.
Zuber, M. T., and Parmentier, E. M. 1984. A Geometric Analysis of Surface Deformation: Implications for the Tectonic Evolution of Ganymede. *Icarus* 60: 200–210.